Proceedings of CONF-MCEE 2026 Symposium: Advances in Sustainable Aviation and Aerospace Vehicle Automation
DOI: 10.54254/2755-2721/2026.KA26063

The Optimization Based on Hydrogen Sulfide-responsive Ratiometric Photoacoustic Probe

Yang Tian

Beijing 101 Middle School, Beijing, China
qingq0639@gmail.com

Abstract. Photoacoustic (PA) imaging relies on molecular systems with strong light absorption and efficient photothermal conversion. In this study, we performed DFT and TD-DFT calculations to investigate how electron-donating and electron-withdrawing substituents influence the photophysical properties of HS-CyBz-based probes. While these substituents modulate the excitation energies of both the thiol-containing reactant and the deprotected product, our results indicate that such a change alone does not significantly enhance the PA signal. These findings suggest that substituent modification is not an effective strategy for optimizing photoacoustic response. Instead, maximizing the difference in π-conjugation between the reactant and product is a more promising design approach for developing efficient PA probes.

Keywords: Photoacoustic imaging, Indocyanine, DFT calculation, Electron-donating and electron-withdrawing group, Hydrogen sulfide

1. Introduction

Hydrogen sulfide (H_2S), the third endogenous gaseous signaling molecule, plays a critical role as a gasotransmitter and is deeply involved in various physiological and pathological processes [1]. At appropriate concentrations, endogenous H_2S exhibits cytoprotective properties, including antioxidative, anti-apoptotic, and anti-inflammatory effects [2]. However, abnormal H_2S accumulation has been linked to the onset and progression of diseases such as Alzheimer's [3], liver cirrhosis [4], inflammation [5], and cancers [6]. Therefore, accurate monitoring of endogenous H_2S is essential for the early diagnosis and treatment of H_2S-related disorders.

Photoacoustic (PA) imaging is a biomedical technique that combines the high contrast of optical imaging with the deep penetration and spatial resolution of ultrasound [7]. Unlike conventional fluorescence imaging, PA imaging overcomes interference from light scattering and absorption in biological tissues [8], making it more suitable for detecting analytes such as reactive oxygen species (ROS) [9], pH [10], enzymes [11], metal ions [12], and H_2S [13].

However, many PA probes rely on single-wavelength signals, which will be easily affected by probe concentration, tissue environment, and light scattering. To overcome these limitations, ratiometric PA imaging, which employs two distinct wavelength signals for internal calibration, has emerged as a promising method to improve detection reliability and signal-to-sound ratio (e.g., [14,15]. Although several ratiometric PA probes for H_2S detection have been developed (e.g.,

© 2026 The Authors. This is an open access article distributed under the terms of the Creative Commons Attribution License 4.0 (https://creativecommons.org/licenses/by/4.0/).

DOI: 10.54254/2755-2721/2026.KA26063

[16,17], challenges such as synthetic complexity, limited spectral shifts, and insufficient multifunctionality persist, restricting their practical applications. In particular, inadequate modulation of excited-state energy levels limits the ratiometric response and accuracy of current PA probes. Therefore, developing H_2S-responsive ratiometric PA probes with improved energy-level tunability and simplified design is critical for achieving precise, quantitative bioimaging.

Previously, Chen et al. developed a heptamethine cyanine-based probe, HS-CyBz, capable of ratiometric PA sensing of H_2S via a reaction-induced spectral shift. This response is induced through nucleophilic substitution by HS^-, followed by keto-enol tautomerization, generating distinct absorption shift for dual-wavelength PA detection (Scheme 1) [18]. The probe demonstrated high sensitivity and a linear increase in the PA ratio (PA825/PA775) with increased H_2S concentration, confirming its potential for quantitative detection (Figure 1).

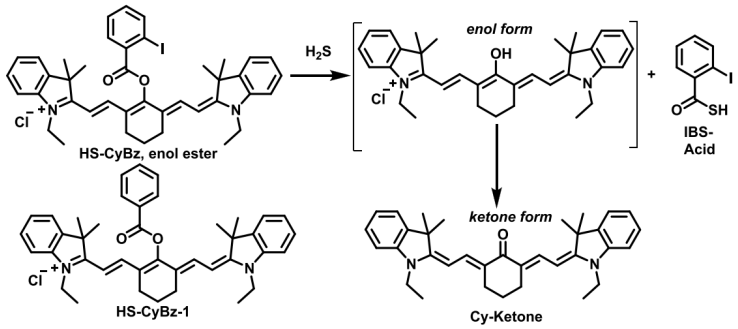

Scheme 1. H_2S-sensing mechanism of HS-CyBz and chemical structure of HS-CyBz-1

Based on the previous work, the present study investigates how substituents with different electronic properties tune the excited-state energy and PA behavior of the HS-CyBz system. Using DFT and TD-DFT calculations, we gained mechanistic insights into how electronic and structural modulation tune energy levels and PA signal output. The computational results suggest that substituent modification is not an effective standalone strategy for optimizing PA response. Instead, maximizing the difference in π-conjugation between the reactant and product is a more robust and promising design approach for developing efficient PA probes. This strategy offers a rational design principle for constructing next-generation PA probes with enhanced performance and molecular precision.

DOI: 10.54254/2755-2721/2026.KA26063

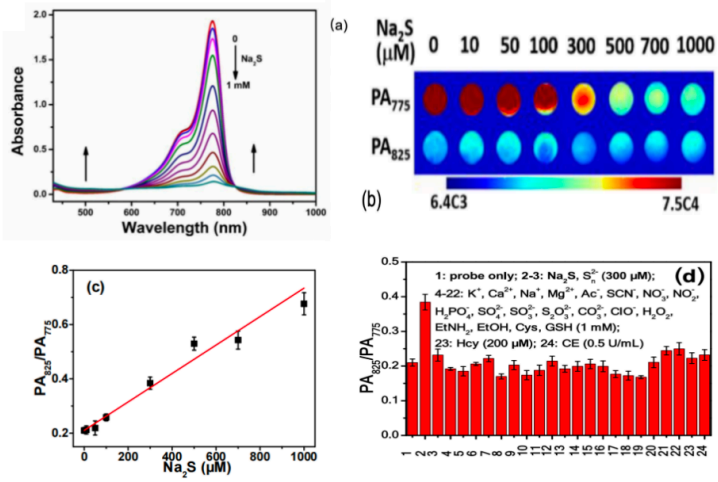

Figure 1. (a). UV-vis absorption spectra of HS-CyBz (10 M) obtained upon titration with Na2S from 0 to 1000 μM in HEPES buffer (20 mM, 20% DMSO, v/v, pH 7.40). Each spectrum was recorded 10 min post Na2S addition. (b). PA image of probe (10 μM) solutions upon Na2S titration (dual-channel mode: λex 775 and 825 nm). (c). PA825/PA775 profile of probe (10 μM) upon Na2S titration (0-1 mM). (d). HS-CyBz (10 μM) in HEPES buffer in the presence of different analytes

2. Methods

All computations were performed using the Gaussian 09 suite of programs [19]. Ground-state molecular geometry optimization was conducted using Density Functional Theory (DFT) with the B_3LYP functional and 6-31G(d) basis set. Excited states and excitation wavelengths were calculated using Time-Dependent Density Functional Theory (TD-DFT) with the M06-2X functional.

3. Results and discussion

Firstly, the ground-state molecular geometry of HS-CyBz was optimized via DFT calculations using the B_3LYP functional and 6-31G(d) basis set. To evaluate the accuracy of excitation wavelength calculations, three common TD-DFT functionals (B_3LYP, M06-2X, and PBE) were tested. As shown in Table 1, M06-2X provided the best alignment with the experimental absorption peak (775 nm) and was selected for all subsequent excited-state calculations.

Table 1. Predicted excitation wavelengths using different TD-DFT methods

Functional	excited wavelength
B_3LYP	778.62 nm
M06-2X	773.51 nm
PBE	790.48 nm

DOI: 10.54254/2755-2721/2026.KA26063

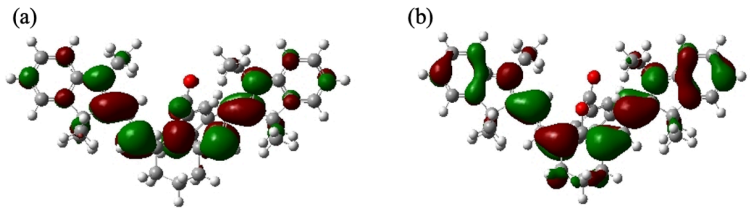

Figure 2. (a) LUMO orbital (b) HOMO orbital of the HS-CyBz

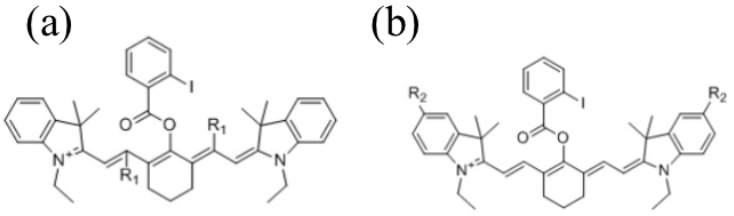

Figure 3. (a) electron withdrawing group (b) electron donating group

To enhance the PA performance of HS-CyBz, several derivatives were designed by introducing electron-withdrawing groups (EWGs) and electron-donating groups (EDGs) at different positions of HS-CyBz. Specifically, three EWGs, nitro (NO_2), cyano (CN), and aldehyde (CHO), were inserted into the conjugated resonance region to influence the LUMO orbital (Figures 2a and 3a). Meanwhile, three EDGs, dimethylamino ($N(CH_3)_2$), hydroxyl (OH), and amino (NH_2), were introduced to the phenyl ring, where the HOMO orbital was localized (Figures 2b and 3b). Due to the molecular symmetry of HS-CyBz, substituents were added to both sides of the molecule for synthetic feasibility.

The excitation wavelengths of the substituted HS-CyBz derivatives, and their corresponding Cy-ketone products were calculated (Table 2). The substituent effects were quantified using Hammett constants (σp), where more positive values indicate stronger electron-withdrawing groups (EWGs) and more negative values indicate stronger electron-donating groups (EDGs). The parameter Δλ represents the wavelength shift between reactant and product. Notably, the dimethylamino-substituted ($N(CH_3)_2$) HS-CyBz exhibited the largest shift (240.45 nm), indicating a substantial narrowing of the HOMO-LUMO gap in the reactant.

DOI: 10.54254/2755-2721/2026.KA26063

Table 2. Excitation wavelength of reactants and products, and the corresponding Δλ

Substituent	Hammett constants σ_p	the excited wavelength of HS-CyBz derivative	the excited wavelength of Cy-ketone derivative	Δλ
NO_2	+0.78	837.97 nm	777.90 nm	60.07 nm
CN	+0.66	471.46 nm	520.22 nm	48.76 nm
CHO	+0.42	793.16 nm	721.31 nm	71.85 nm
$N(CH_3)_2$	-0.83	759.46 nm	519.01 nm	240.45 nm
OH	-0.37	451.09 nm	514.28 nm	63.19 nm
NH_2	-0.66	451.58 nm	517.85 nm	66.27 nm

However, compared with unsubstituted HS-CyBz and Cy-ketone, of which absorption peak are at 775 nm and 525 nm, respectively, most substituted derivatives demonstrated significantly smaller wavelength shifts, indicating that stronger substituent effect did not translate into PA advantages. The substituents either narrowed the reactant's conjugation leading to a blue shift, or expanded the product's conjugation leading to a red shift, both of which reduced the wavelength shift between reactant and product. The only exception was dimethylamino ($N(CH_3)_2$), where steric hindrance from the methyl groups weakened conjugation between the amine and phenyl ring, preserving an electronic structure similar to unsubstituted HS-CyBz and Cy-ketone. The distinct absorption wavelengths of HS-CyBz and Cy-ketone arise from differences in their π-conjugation systems. While Cy-ketone exhibits localized conjugation limited to two isolated phenyl rings, HS-CyBz possesses a more extended π-system, resulting in a pronounced red shift in absorption wavelength.

4. Conclusion

In this study, the effects of electron-donating and electron-withdrawing substituents on the photophysical properties of HS-CyBz derivatives was evaluated using TD-DFT calculations. While substituents influenced the excitation energies of both reactant and product forms, strong electron-donating or -withdrawing groups did not consistently enhance the PA signal.

These findings suggest that tuning the substituent’s electronic properties alone may not be an effective strategy to improve the PA signal. Instead, maximizing the difference in the extent of conjugation between the reactant and product, thereby modulating their respective absorption profiles, could be a more reliable approach for optimizing PA contrast in molecular designs.

Acknowledgements

I would like to express my gratitude to all those who offer help for my thesis. First and foremost, my deepest gratitude goes to the stage of Yuanpei Young Scholar program and my supervisors, Prof. Juan Yang and Dr. Runting Fang, for their comprehensive and continuous guidance. They provide me with abundant suggestions and priceless criticisms for my research. My sincere thanks also go to

DOI: 10.54254/2755-2721/2026.KA26063

the academic fields. All of the previous research offers me inspiration and encouragement, which accompany me throughout my research process. I feel indebted to my parents, with their mental and material support, I could finish my research very well. Finally, my thanks should be sent to all my classmates for their endless support and warm hearts, making me feel like living in a big united family.

References

[1] Szabo, C. Gasotransmitters in Cancer: From Pathophysiology to Experimental Therapy. Nat. Rev. Drug Discov. 2016, 15 (3), 185–203. https: //doi.org/10.1038/nrd.2015.1.
[2] Zhao, Y.; Matthew. M, C.; Michael D., P. Fluorogenic Hydrogen Sulfide (H2S) Donors Based on Sulfenyl Thiocarbonates Enable H2S Tracking and Quantification - Chemical Science (RSC Publishing). Chem. Sci. 2019. https: //doi.org/10.1039/C8SC05200J.
[3] Kshirsagar, viplav vitthal; Thingore, C.; Juvekar, A. Hydrogen Sulfide Alleviates Lipopolysaccharide-induced Memory Impairment, Neurodegeneration and Neuroinflammation in Swiss Albino Mice - Kshirsagar - 2020 - Alzheimer's & Dementia - Wiley Online Library.
[4] Fiorucci, S.; Antonelli, E.; Mencarelli, A.; Orlandi, S.; Renga, B.; Rizzo, G.; Distrutti, E.; Shah, V.; Morelli, A. The Third Gas: H2S Regulates Perfusion Pressure in Both the Isolated and Perfused Normal Rat Liver and in Cirrhosis*. Hepatology 2005, 42 (3), 539. https: //doi.org/10.1002/hep.20817.
[5] Bindu.D Paul; Solomon H. Snyder. H2S Signalling through Protein Sulfhydration and beyond | Nature Reviews Molecular Cell Biology. Nat. Rev. Drug Discov.
[6] Weiyu Chen; Dalong Ni; Rosenkrans, Z. T.; Tianye Cao; Weibo Cai. Smart H2S-Triggered/Therapeutic System (SHTS)-Based Nanomedicine - Chen - 2019 - Advanced Science - Wiley Online Library.
[7] Attia, A. B. E.; Balasundaram, G.; Moothanchery, M.; Dinish, U. S.; Bi, R.; Ntziachristos, V.; Olivo, M. A Review of Clinical Photoacoustic Imaging: Current and Future Trends. Photoacoustics 2019, 16, 100144. https: //doi.org/10.1016/j.pacs.2019.100144.
[8] Zhang, Y.; Fang, J.; Ye, S.; Zhao, Y.; Wang, A.; Mao, Q.; Cui, C.; Feng, Y.; Li, J.; Li, S.; Zhang, M.; Shi, H. A Hydrogen Sulphide-Responsive and Depleting Nanoplatform for Cancer Photodynamic Therapy. Nat. Commun. 2022, 13 (1), 1685. https: //doi.org/10.1038/s41467-022-29284-7.
[9] Yang, Z.; Dai, Y.; Yin, C.; Fan, Q.; Zhang, W.; Song, J.; Yu, G.; Tang, W.; Fan, W.; Yung, B. C.; Li, J.; Li, X.; Li, X.; Tang, Y.; Huang, W.; Song, J.; Chen, X. Activatable Semiconducting Theranostics: Simultaneous Generation and Ratiometric Photoacoustic Imaging of Reactive Oxygen Species In Vivo. Adv. Mater. 2018, 30 (23), 1707509. https: //doi.org/10.1002/adma.201707509.
[10] Chen, Q.; Liu, X.; Chen, J.; Zeng, J.; Cheng, Z.; Liu, Z. A Self-Assembled Albumin-Based Nanoprobe for In Vivo Ratiometric Photoacoustic pH Imaging. Adv. Mater. 2015, 27 (43), 6820–6827. https: //doi.org/10.1002/adma.201503194.
[11] Lei, S.; Zhang, J.; Blum, N. T.; Li, M.; Zhang, D.-Y.; Yin, W.; Zhao, F.; Lin, J.; Huang, P. In Vivo Three-Dimensional Multispectral Photoacoustic Imaging of Dual Enzyme-Driven Cyclic Cascade Reaction for Tumor Catalytic Therapy. Nat. Commun. 2022, 13 (1), 1298. https: //doi.org/10.1038/s41467-022-29082-1.
[12] Steinbrueck, A.; Karges, J. Metal Complexes and Nanoparticles for Photoacoustic Imaging. ChemBioChem 2023, 24 (14), e202300079. https: //doi.org/10.1002/cbic.202300079.
[13] Ben Shi; Xianfeng Gu; Qiang Fei; Chunchang Zhao. Photoacoustic Probes for Real-Time Tracking of Endogenous H 2 S in Living Mice - Chemical Science (RSC Publishing) DOI: 10.1039/C6SC04703C. R. Soc. Chem.
[14] Xiao, H.; Wu, C.; Li, P.; Gao, W.; Zhang, W.; Zhang, W.; Tong, L.; Tang, B. Ratiometric Photoacoustic Imaging of Endoplasmic Reticulum Polarity in Injured Liver Tissues of Diabetic Mice. 2017. https: //doi.org/10.1039/C7SC02330H.
[15] Kang Zhu; Xuan Zhang; Ying Wu; Jibin Song. Ratiometric Optical and Photoacoustic Imaging In Vivo in the Second Near-Infrared Window | Accounts of Chemical Research. Acc. Chem. Res.
[16] Rongrong Wu; Zhongxiang Chen; Hongqi Huo; Lanlan Chen*; Lichao Su; Xuan Zhang; Ying Wu; Zhicun Yao; Shenggan Xiao; Wei Du*; Jibin Song*. Ratiometric Detection of H2S in Liver Injury by Activated Two-Wavelength Photoacoustic Imaging | Analytical Chemistry. Anal. Chem.
[17] Ma, T.; Zheng, J.; Zhang, T.; Xing, D. Ratiometric Photoacoustic Nanoprobes for Monitoring and Imaging of Hydrogen Sulfide in Vivo. Nanoscale 2018, 10 (28), 13462–13470. https: //doi.org/10.1039/C8NR03445A.
[18] Chen, Z.; Mu, X.; Han, Z.; Yang, S.; Zhang, C.; Guo, Z.; Bai, Y.; He, W. An Optical/Photoacoustic Dual-Modality Probe: Ratiometric in/Ex Vivo Imaging for Stimulated H2S Upregulation in Mice. J. Am. Chem. Soc. 2019. https:

DOI: 10.54254/2755-2721/2026.KA26063

//doi.org/10.1021/jacs.9b09181.
[19] Gaussian 09 Citation | Gaussian.com. https: //gaussian.com/g09citation/ (accessed 2025-06-08).